Inorganic Chemistry

Article

pubs.acs.org/IC

Synthesis and Characterization of Low-Generation Polyamidoamine (PAMAM) Dendrimer–Sodium Montmorillonite (Na-MMT) Clay Nanocomposites

Amila U. Liyanage, Esther U. Ikhuoria,† Adeniyi A. Adenuga, Vincent T. Remcho, and Michael M. Lerner*

Department of Chemistry, Oregon State University, Corvallis, Oregon 97331-4003, United States

Supporting Information

ABSTRACT: Polymer–inorganic nanocomposites are a recently developed class of materials that have altered physical or chemical properties with respect to the pure polymer, inorganic host, or their micro- and macrocomposites. Lower generation (G0.0–2.0) polyamidoamine (PAMAM) dendrimer/sodium montmorillonite (Na-MMT) nanocomposites were synthesized in a solution-phase exfoliation adsorption reaction. These are the first reports of the G0.0/ and G1.0/Na-MMT nanocomposites and of a structurally-ordered G2.0/Na-MMT. The materials were characterized using powder X-ray diffraction (PXRD), thermogravimetric analysis (TGA), and Fourier transform infrared spectroscopy (FTIR). PAMAM characteristics at acidic and basic aqueous media were studied using capillary zone electrophoresis (CZE). Pseudospherical PAMAM dendrimers in aqueous medium attain a highly flattened conformation within the confined space between MMT sheets upon nanocomposite formation. The nanocomposite structure depends on the PAMAM generation and the starting dendrimer/organic composition. G0.0 always forms monolayer structures (d = 0.42 nm), while G2.0 forms monolayer structure, mixed phase, and bilayer structures (d = 0.84 nm) at lower, intermediate, and higher organic content, respectively, showing an interesting monolayer to bilayer transition. G1.0 showed an intermediate behavior, with monolayer to mixed-phase transition at the reactant ratios studied. This monolayer arrangement of PAMAM/clay nanocomposites is reported for the first time. Maximum organic contents of G0.0 monolayer and G2.0 bilayer nanocomposites were ∼7% and ∼14%, respectively. Gallery expansions were similar to those observed with linear polymer intercalates, but the packing fractions (0.31–0.32) were 2–3 times lower. At acidic pH, the nanocomposites forming only monolayer structures are obtained, indicating a stronger electrostatic attraction between MMT and protonated PAMAM, and these nanocomposites formed more slowly and were more ordered. Na^+ ions play a significant role in nanocomposite formation. At high pH, PAMAMs show high mobility, ζ potential, and surface charge densities due to Na^+ complexation in solution. FTIR data indicates that both Na-MMT and PAMAM structural units are preserved in the nanocomposites obtained.

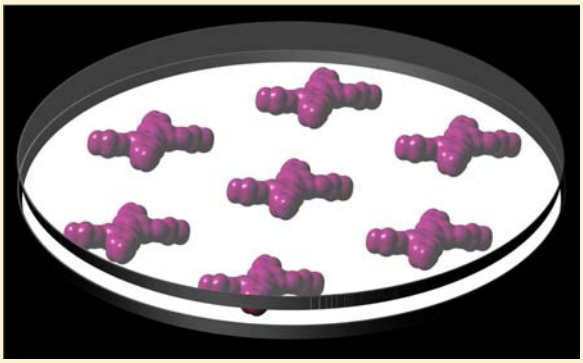

INTRODUCTION

Polymer–inorganic nanocomposites are a recently developed class of materials with at least one dimension of the phase combination in the nanometer range. Depending on the overall dimensionality, there are several types of nanocomposites; a prominent example is where two-dimensional (layered) inorganic structures incorporate or are dispersed into polymers.[1] In these polymer-containing layered nancomposites, some polymers studied include poly(ethylene oxide) (PEO),[2−4] linear polyethylenimine (LPEI),[4,5] poly(vinyl alcohol) (PVOH),[4,6] poly(vinyl pyrrolidone) (PVPyr),[4] and polyaniline (PANI)[7] polymers; the inorganic structures include clays,[2,3] transition metal oxides, sulfides, selenides,[3,5,7] or phosphorus trisulfides[4,5] and layered double hydroxides.[8] Depending on the nature and relative composition of these constituents and also on the preparative method employed, the nanocomposites may form as intercalation compounds (ordered) or as exfoliated (amorphous) structures.[9] Some preparative methods include exfoliation–adsorption,[2,3] in situ intercalative polymerization,[10] melt intercalation,[11,12] and template synthesis.[4] A major reason for the growing interest in these nanocomposite materials is their remarkably changed mechanical, thermal, optical, or physicochemical properties with respect to the constituent phases or conventional microcomposites.[1] Specific improvement for applied materials include increased moduli, tensile stress, thermal stability, and flame retardancy, decreased gas permeability, and enhanced thermal stability of the ionic conductivity.[1,13]

Sodium montmorillonite, $Na_x(Al_{4-x}Mg_x)Si_8O_{20}(OH)_4$ (Na-MMT), is a smectite belonging to the structural family known as 2:1 phyllosilicates, which has layers with central alumina or magnesia octahedra bound and covered by silica surfaces.[1,13] These anionic sheets are stacked with monovalent cation (Na^+)

Received: January 25, 2013
Published: March 29, 2013

   dx.doi.org/10.1021/ic400198g | Inorg. Chem. 2013, 52, 4603–4610

residing between them. The stacking repeat for the anhydrous structure is 0.96 nm; ion exchange or co-intercalation of molecules, surfactants, or polymers between the layers can result in expansion of the layer repeat or delamination of the sheets into solution.[5,14,15]

Dendrimers are monodisperse macromolecules with a regular and highly branched three-dimensional architecture, which consists of three basic components, an initiator core, interior zones comprising cascading tiers of branches with radial connectivity to the initiator core, and an exterior surface with terminal groups.[16,17] Higher generation dendrimers add to the interior zone tiers. Polyamidoamines (PAMAMs) are the first synthetic dendrimers, with potential applications in drug or gene delivery, sensors, and nanoparticle synthesis.[18−21] Although dendrimers can have functional groups similar to those in linear polymers, the net connectivity contrasts with that of linear polymers and provides an opportunity to evaluate the effect of organic component on nanocomposite structure and the gallery composition of intercalated nanocomposites.

Previous studies have reported nanocomposites combining hyperbranched polymers,[22,23] higher-generation PAMAMs,[24] dendrons,[25] or dendritic quaternary ammoniums[26] with smectite clays including montmorillonite[22−26] or kaolinite.[27] Those reports indicated very large gallery expansions,[22,25,26] both pure and mixed-phase intercalated nanocomposites,[22,24−26] and exfoliated nanocomposites.[22]

Ratanarat et al.[15] have reported the only lower generation PAMAM/Na-MMT nanocomposite, an exfoliated nanocomposite of generation 2.0 (G2.0) PAMAM and Na-MMT. Alongi et al.[24] have reported the synthesis of higher generation (G4.0−7.0) PAMAM/Na-MMT nanocomposites. Here we report the first systematic compositional study on the synthesis and characterization of lower generation PAMAM/Na-MMT nanocomposites and clarify the adsorbed monolayer/bilayer arrangements that occur in dendrimer nanocomposite galleries.

EXPERIMENTAL SECTION

Reagents. Polyamidoamine (PAMAM) aqueous solutions (∼16% w/w, Dendritech), sodium montmorillonite (Na-MMT) (SWy-2, Clay Minerals Society), HCl (36.5−38.0%, EMD), H_3PO_4 (85%, Mallinckrodt), Na_2HPO_4 (ACS grade, Mallinckrodt Baker), NaOH (ACS grade, Mallinckrodt), NaCl (ACS grade, Mallinckrodt), montmorillonite K 10 (Sigma-Aldrich), and $AgNO_3$ (ACS grade, Alfa Aesar) were purchased and used without further purification.

Syntheses. Aqueous solutions of PAMAM (0.01−0.08 g, 10.00 mL, pH 11−12) were added dropwise to aqueous suspensions of Na-MMT (0.1000 g, 10.00 mL, pH 5−6). Cloudy or powder-like white particles were visible within a few seconds to several minutes of combining the reactants. The suspensions had pH = 10−11 and were stirred vigorously overnight at room temperature. The white precipitate was collected after centrifugation for 10 min, washed twice with deionized (DI) water, and then dried under vacuum at 60 °C for 18 h. Some reactions were performed at ambient temperature and some at 60 °C.

In another set of nanocomposite syntheses, the PAMAM aqueous solutions were adjusted to pH = 2−3 using 1 M HCl prior to addition of the Na-MMT suspension. Higher temperatures (50, 80 °C) were also utilized for some of these syntheses. These obtained products were washed repeatedly until no precipitate formed on reaction with dilute $AgNO_3$ (aq).

Samples are labeled below based on the reacted g/g PAMAM/Na-MMT ratios and PAMAM generation. For example, the sample obtained by reaction of 0.010 g of generation 0.0 PAMAM with 0.1000 g of suspended Na-MMT is labeled "0.1G(0.0)". For reactions carried out at temperatures other than ambient temperature and pHs other than pH = 10−11, the temperature (in °C) and pH are also indicated, for example "0.6G(2.0)-50-2".

Analytical Methods. Powder XRD (PXRD) patterns from 2° to 15° 2θ were obtained on a Rigaku Miniflex II diffractometer, using Ni-filtered Cu Kα radiation at a scan rate of 1° min^{-1} and step size of 0.020° 2θ. A modified Scherrer equation[4] was used to determine crystallite size (L) for the prepared nanocomposites:

$$L_{hkl} = \frac{0.9\lambda}{\cos\theta_{hkl}[\Delta^2(2\theta_{hkl}) - \Delta^2(2\theta_{hkl})_{std}]^{1/2}} \quad (1)$$

where λ = 0.15418 nm, $\Delta(2\theta_{hkl})$ = full width at half-maximum (in radians), and θ_{hkl} = diffraction angle. A Si(m) powder standard was employed for these measurements.

Thermogravimetric (TGA) analyses were performed under Ar flow (20 mL/min) using a Shimadzu TGA-50 analyzer. Approximately 10−15 mg of sample was placed into an open platinum pan and heated from ambient to 600 °C at 5 °C/min.

Capillary zone electrophoresis was performed to determine migration times using an HP ^{3D}CE instrument equipped with a UV detector, using a 75 μm inner diameter, 58.5 cm long fused silica capillary (50.0 cm to the detection window). New capillaries were sequentially conditioned by flushing with methanol (30 min), water (Milli-Q) (5 min), 1.0 M NaOH (30 min), water (5 min), and finally the background electrolyte (BGE) for 30 min. As preconditioning, the capillary was flushed with 0.1 M NaOH (3 min), water (1 min), and BGE (4 min). As postconditioning, the capillary was flushed with water (1 min). Background electrolytes used were 100 mM H_3PO_4, pH adjusted to 2.7, and 50 mM Na_2HPO_4, pH adjusted to 10.9 with NaOH. Ionic strengths of BGEs were adjusted to ∼0.16 mol L^{-1} using NaCl. Samples were prepared by freshly dissolving in H_3PO_4 or Na_2HPO_4, and the sample was adjusted to the pH and the ionic strength of BGE, using NaOH and NaCl, respectively. Migrations were accomplished at applied voltages of +15 kV (pH 2.7) and +18 kV (pH 10.9). The capillary was thermostatted at 25 °C (pH 2.7) or 30 °C (pH 10.9). Solutions were injected hydrodynamically at 50 mbar for 5 s. Direct detection was employed at a wavelength of 210 nm.

The dimensionless mobility (μ_0') of the dendrimers was calculated using

$$\mu_0' = \frac{\mu_0 3\eta e}{2\xi\xi_0 kT} = \frac{lL}{Vt_m}\frac{3\eta e}{2\xi\xi_0 kT} \quad (2)$$

where l is the effective length, L is the total length, V is the voltage, t_m is the migration time, μ_0 is the electrophoretic mobility, ξ is the dielectric constant of water (80.5), ξ_0 is the dielectric permittivity of the vacuum, k is the Boltzmann constant, T is the temperature in kelvin, η is the viscosity, and e is charge of the electron. Dimensionless ζ potentials and charge distribution functions (I_0) were obtained using numerical solutions published by Wiersema et al.[28] and Loeb et al.[29] Zeta potential (ζ) and surface charge densities (σ) were calculated according to the following empirical formulas:[30]

$$\zeta = \zeta'\frac{kT}{e} \quad (3)$$

$$\sigma = 5.8718I^{1/2}I_0 \times 10^{-2} \quad \text{C/m}^2 \quad (4)$$

IR spectra were taken using a Nicolet iS10 FT-IR spectrometer with an ATR sample cell, using background corrections for air and collection geometry. Aqueous PAMAM solutions were preconcentrated at 80 °C before collecting spectra. Diamond and Ge ATR cells were used for liquid and solid samples, respectively.

van der Waals volumes of PAMAM dendrimers (G 0.0, 1.0, and 2.0) were calculated based on Bondi radii using a method termed "Atomic and Bond Contributions of van der Waals volume" (VABC).[31] Packing fractions were calculated[4] using

$$\text{packing fraction} = [(ZnV_{vdw})/(ab\Delta d)] \quad (5)$$

where a = 0.517 and b = 0.894 nm are Na-MMT unit cell parameters,[32] Δd = interlayer expansion = d_i − 0.96 nm, where d_i and 0.96 nm are interlayer repeat distances of the nanocomposite and

dx.doi.org/10.1021/ic400198g | Inorg. Chem. 2013, 52, 4603−4610

anhydrous Na-MMT, respectively, Z = the number of Na-MMT formula units per cell = 1, n = the number of PAMAM molecules per Na-MMT formula unit, and V_{vdw} = van der Waals volume of the PAMAM molecule.

Energy optimization of the gas-phase highly flattened and pseudospherical G0.0 PAMAM molecules was performed using DFT B3LYP method with 6-31G(d) basis set using Gaussian 09W software.

RESULTS AND DISCUSSION

As shown in Figure 1, G0.0 nanocomposites show interlayer repeat spacings (d) of 1.37−1.38 nm. Since the interlayer

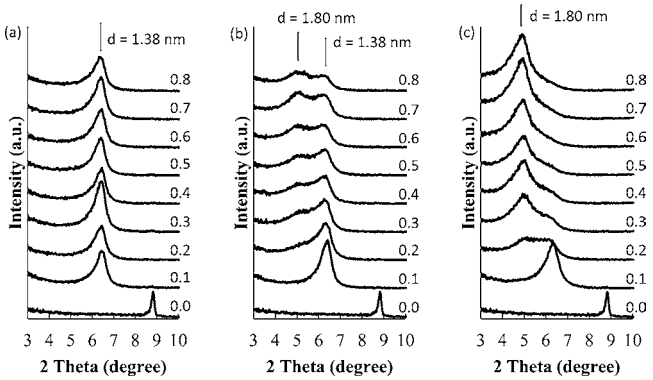

Figure 1. PXRD patterns for (a) G(0.0), (b) G(1.0), and (c) G(2.0) PAMAM/Na-MMT nanocomposites. The reactant ratios (g/g PAMAM/Na-MMT) are indicated.

repeat distance of anhydrous Na-MMT is 0.96 nm, these spacings correspond to an interlayer expansion (Δd) of 0.41−0.42 nm. For G2.0 PAMAM, the nanocomposites obtained show a compositional effect with a more expanded phase, with Δd = 0.83−0.84 nm appearing only at compositions richer in dendrimer content. Except for 0.1G(1.0), which shows only the Δd = 0.42 nm phase, G(1.0) PAMAM nanocomposites show both these expanded phases, with the more expanded phase increasing in relative intensity at higher starting dendrimer compositions. These observations differ from Ratanarat et al.[15] report on exfoliated G2.0 PAMAM/Na-MMT nanocomposite. But the observed d values and the corresponding Δd calculated are comparable to those obtained by Alongi et al. with higher generation (G4.0−7.0) PAMAM and Na-MMT (d = 1.74−1.93 nm; Δd = 0.78−0.97 nm)[24] and Amin et al. with a hyperbranched polymer and Na-MMT (d = 1.397, 1.705 nm, Δd = 0.437, 0.745 nm).[33]

As will be discussed below, the two expanded phases obtained in our compositional studies contain galleries comprising ∼0.4 nm thick PAMAM mono- or bilayers. The dendrimers are strongly adsorbed onto the clay surface and do not structurally resemble their solution-phase conformations.

TGA data for these nanocomposites show four mass loss regions, also indicated by four peaks in the derivative (DTG) curves at <100, 210, 350, and >590 °C. (Figure 2). These are attributed, respectively, to loss of intercalate water, a two-step degradation of PAMAM, and finally the degradation of the MMT sheet structure to liberate H_2O. Alongi et al.[24] observed a decomposition step around 200 °C that was ascribed to nonintercalated PAMAM. Since native PAMAM degrades in a single step around 300 °C, the lower temperature loss was attributed to a previously reported catalytic effect for organic decomposition on clays, for example, with quaternary ammonium/MMT intercalated composites.[34] Because the

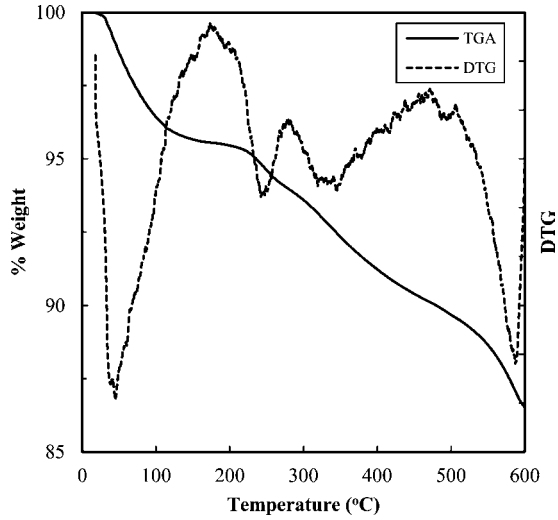

Figure 2. Mass loss and differential plots for 0.6G(1.0)-2 PAMAM/Na-MMT nanocomposite.

PAMAM content in our products does not change significantly upon extended washing, and many different starting compositions resulted in similar mass losses, the presence of a significant fraction of nonintercalated PAMAM residue appears unlikely, and both mass loss steps at 210 and 350 °C are ascribed to the decomposition of intercalated PAMAM.

Table 1 compares interlayer distance (d), interlayer expansion (Δd), composition, packing fraction, and crystallite size (L) of different nanocomposites obtained in this study.

Depending on the relative charge densities of the clay host and guest, different intercalate arrangements can arise, including monolayers, lateral bilayers, pseudotrilayers, or an inclined paraffin-like structure.[1,35] Linear polymer/Na-MMT and linear alkyl ammonium/Na-MMT nanocomposites have shown monolayer intercalate structures that transition to bilayers with increasing intercalate content.[2,14] For all the obtained materials, only two interlayer expansions were observed, ∼0.42 and ∼0.84 nm, as shown in Figure 3 and Table 1. A plot of organic mass content for the G0.0 nanocomposites reaches a plateau at ∼7% and that for G2.0 at ∼14% (Table 1, Figure 4). Where two intercalated phases have both gallery dimensions and organic compositions in a 2:1 ratio, a monolayer/bilayer structure model is strongly indicated. Because only mixed phases and no intermediate values for interlayer expansion are observed, a monolayer to bilayer transition is observed with increasing PAMAM content for G1.0 and G2.0.

The interlayer distances and interlayer expansion values for PAMAM/Na-MMT nanocomposites were also comparable to previously reported polymer/Na-MMT nanocomposites (Table 2), supporting the proposed monolayer and bilayer models. Although PVOH/Ca-MMT nanocomposites showed higher interlayer expansion values than with typical polymer monolayers, Carrodo et al.[6] note that extensive drying *in vacuo* at 65 °C also results in $\Delta d \approx$ 0.4 nm.

These small dimensions require a highly flattened dendrimer conformation within the galleries. Compared with a solution diameter of >1.5 nm,[36,37] the maximum thickness for the dendrimers in the mono- and bilayers is ∼0.4 nm for the nanocomposites we report. The strong adsorption of the dendrimers on the clay surfaces, coupled with the favorable lattice enthalpy for smaller expansions, result in minimum

dx.doi.org/10.1021/ic400198g | Inorg. Chem. 2013, 52, 4603−4610

Table 1. Structural and Compositional Data for PAMAM/Na-MMT Nanocomposite Products Obtained Using PXRD (d and Δd) and TGA (Organic Mass %) and Derived Packing Fractions and Crystallite Sizes (L)

sample	reactant ratio (g/g PAMAM/Na-MMT)	condition, temp[a]/pH	phase	d (nm)	Δd (nm)	organic mass %	packing fraction	L (nm)
0.1G(0.0)	0.1	RT/10−11	monolayer	1.38	0.42	5.6	0.23	129
0.2G(0.0)	0.2			1.37	0.41	6.5	0.28	126
0.3G(0.0)	0.3			1.38	0.42	6.6	0.28	128
0.4G(0.0)	0.4			1.37	0.41	6.6	0.28	130
0.5G(0.0)	0.5			1.38	0.42	7.2	0.30	128
0.6G(0.0)	0.6			1.37	0.41	7.4	0.31	126
0.7G(0.0)	0.7			1.38	0.42	7.3	0.31	125
0.8G(0.0)	0.8			1.38	0.42	7.5	0.31	122
0.1G(1.0)	0.1	RT/10−11	monolayer	1.38	0.42	5.6	0.23	127
0.2G(1.0)	0.2		mixed	1.39, 1.74	0.43, 0.78	8.2	[b]	[b]
0.3G(1.0)	0.3			1.42, 1.74	0.46, 0.78	9.1		
0.4G(1.0)	0.4			1.39, 1.78	0.43, 0.82	9.2		
0.5G(1.0)	0.5			1.40, 1.76	0.44, 0.80	10.2		
0.6G(1.0)	0.6			1.41, 1.75	0.45, 0.79	10.2		
0.7G(1.0)	0.7			1.72, 1.42	0.76, 0.46	10.7		
0.8G(1.0)	0.8			1.77, 1.41	0.81, 0.45	11.0		
0.1G(2.0)	0.1	RT/10−11	monolayer	1.39	0.43	5.3	0.21	115
0.2G(2.0)	0.2		mixed	1.77, 1.42	0.81, 0.46	10.4	[b]	[b]
0.3G(2.0)	0.3			1.80, 1.42	0.84, 0.46	11.7		
0.4G(2.0)	0.4			1.79, 1.42	0.83, 0.46	13.1		
0.5G(2.0)	0.5			1.79, 1.42	0.83, 0.46	13.8		
0.6G(2.0)	0.6		bilayer	1.80	0.84	14.1	0.32	116
0.7G(2.0)	0.7			1.80	0.84	13.9	0.31	108
0.8G(2.0)	0.8			1.80	0.84	14.5	0.33	103
0.6G(0.0)-2	0.6	RT/2−3	monolayer	1.36	0.40	6.6	0.29	141
0.6G(1.0)-2	0.6			1.36	0.40	6.6	0.29	145
0.6G(2.0)-50−2	0.6	50 °C/2−3		1.36	0.40	7.9	0.35	141
0.6G(2.0)-80−2	0.6	80 °C/2−3		1.36	0.40	7.1	0.31	144
0.3G(0.0)-60	0.3	60 °C/10−11	monolayer	1.37	0.41	6.2	0.26	133
0.3G(1.0)-60	0.3		mixed	1.40, 1.80	0.44, 0.84	8.5	[b]	[b]
0.3G(2.0)-60	0.3			1.81, 1.41	0.85, 0.45	11.4		

[a]RT = ambient temperature [b]Not applicable.

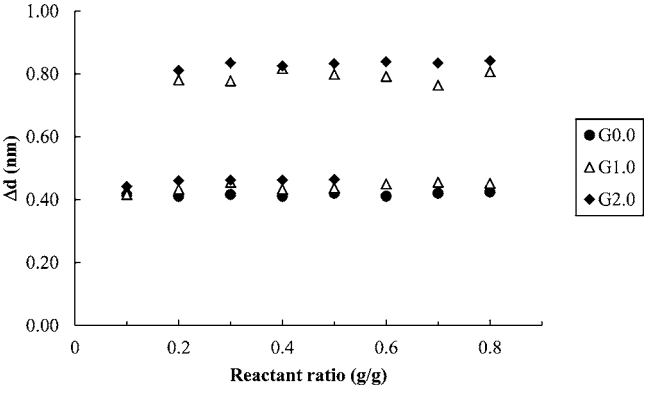

Figure 3. Interlayer expansion variation with reactant ratios, PAMAM/Na-MMT g/g, at room temperature and pH 10−11.

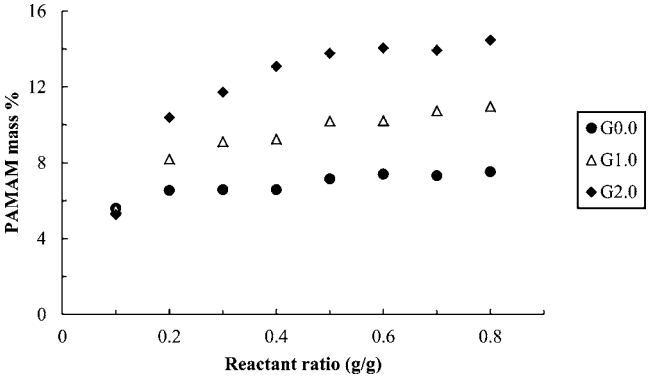

Figure 4. Dendrimer mass % variation with reactant ratios, PAMAM/Na-MMT g/g, at room temperature and pH 10−11.

gallery expansions. The larger dendrimers show more favorability for the bilayer structure, most likely because their greater footprint in adsorbed form requires a larger intercalate volume for charge compensation of the anionic host.

Previous studies have shown altered PAMAM conformations due to interfacial or host−guest interactions. Lower generation (G0.0−G3.0) PAMAM dendrimers with an ethylenediamine core have an ellipsoidal shape, whereas the higher generation dendrimers (G4.0−G10.0) have a roughly spherical shape.[36,38] A significant flattening of dendrimers has been observed on mica,[39,40] Au,[41] and Pt[42] substrates; Hierlemann et al. provided evidence for 0.5−0.8 nm thick G4.0 dendrimers on a Au surface.[41] Even the highly branched net PAMAM, at least for the lower generations, can compress into a highly flattened conformation with minimum dimension comparable to those observed in the mono- and bilayers obtained.

To further explore the feasibility for such highly flattened structures, a PAMAM G0.0 dendrimer was structurally

dx.doi.org/10.1021/ic400198g | Inorg. Chem. 2013, 52, 4603−4610

Table 2. Compositional and Packing Data for Polymer/A-MMT Nanocomposites

nanocomposite	phase	d_{001} (nm)	Δd (nm)	organic mass %[a]	packing fraction[a]	ref
PEO/Na-MMT	monolayer	1.37	0.41	13	0.67	2
PEO/Na-MMT	bilayer	1.77	0.81	23	0.68	2
PEI/Na-MMT	monolayer	1.38	0.42	18	0.93	5
PVOH/Ca-MMT (heated)		1.70	0.74	10.3	0.24	6
PVOH/Ca-MMT		1.55	0.59	8	0.23	6

[a]Calculated from the compositional and structural data provided in the references indicated.

optimized with flattened conformation of only 0.38 nm using Gaussian 09W (see Figure 5). While the flattened model may not correspond to the precise conformation of the dendrimer intercalates, the result does support the feasibility of such PAMAM conformations in the obtained nanocomposites. We calculate the flattened conformation energy of PAMAM G0.0 to be ~100−200 kcal/mol higher than the pseudospherical conformation. However, these are gas-phase calculations and do not account for the real synthetic conditions, where both solvation and clay surface interactions are important.

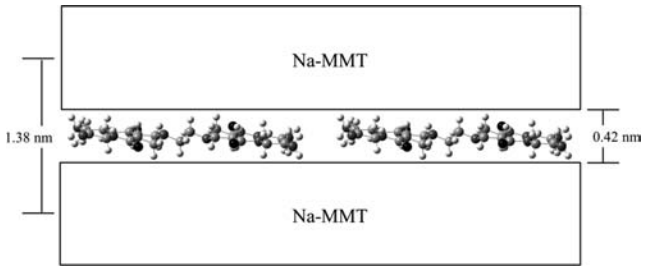

Figure 5. A structural model for the G0.0 monolayer nanocomposites. (H, white; O, black; C, light gray; N, dark gray).

Under acidic synthetic conditions (pH = 2−3), all the obtained nanocomposites show only intercalate monolayers. Figure 6 compares PXRD patterns obtained under acidic and basic conditions for the different PAMAM generations. As shown in Table 1, the interlayer expansion for acidic syntheses decreases slightly, by ~0.02 nm, while the crystallite domain size increases by ~10−15 nm. Under these acidic conditions, the terminal primary amines on PAMAM ($pK_a \approx 9-10$)[43−45] are protonated, and the cationic dendrimers must ion exchange with Na^+ ions in Na-MMT. The slightly smaller interlayer expansion suggests that the protonated PAMAM bonds strongly via electrostatic interaction with the anionic MMT sheets. A similar observation was reported by Alongi et al.[24] using protonated G4.0 PAMAM, where a smaller interlayer expansion occurs than for materials prepared at higher pH.

The increase in crystallite size at lower pH can be attributed to the observed slower reaction rates. For example, under acidic conditions, a flocculate does not appear at ambient temperature with G2.0 PAMAM. At 50 °C, particles appear after reaction for 30 min, and at 80 °C they appear after 10 min. Elevated temperature also increases the nanocomposite yield, although the yield remains lower than that under basic conditions. The slower reaction kinetics may again be associated with an ion exchange process required for a positively charged dendrimer.

When reactions are performed where a protonated montmorillonite, K10 (H-MMT) is substituted for Na-MMT, no dendrimer intercalation is observed. This difference implicates Na^+ in the intercalation reaction, either via ion exchange or dendrimer complexation.

To study the effect of synthesis temperature, 0.3 g/g PAMAM/Na-MMT nanocomposites with all G0.0, G1.0, and G2.0 PAMAM were prepared at ambient temperature and at 60 °C. The obtained gallery dimensions (Table 1, Δd) and relative phase contents for mixed phases as indicated by PXRD reflection intensities (Figure 1S, Supporting Information) did not change significantly at higher temperature. However, the organic mass contents were lower at higher temperature (Table 1), which suggests that the higher rate of nanocomposite formation prevents efficient packing of the expanded galleries with PAMAM.

For G0.0 nanocomposites, an increase of PAMAM packing fraction was also observed at higher initial dendrimers ratios (Figure 7, left). G2.0 nanocomposites that formed with higher organic loading are more tightly clustered (Figure 7, right) indicating less effect of starting composition on product composition. It is very clear that there are two structures having similar packing fractions at full loading (0.31 for the monolayer, and 0.33 for the bilayer). H_2O may partially fill the available volume in the galleries; water content was not considered in the packing fraction calculation because the water contents are highly variable and depend in part on sample history. For comparison, packing fractions of ~0.67−0.68 can be deduced from reported data for PEO/Na-MMT mono- and bilayer intercalate structures[2] and of 0.93 for PEI/Na-MMT,[5]

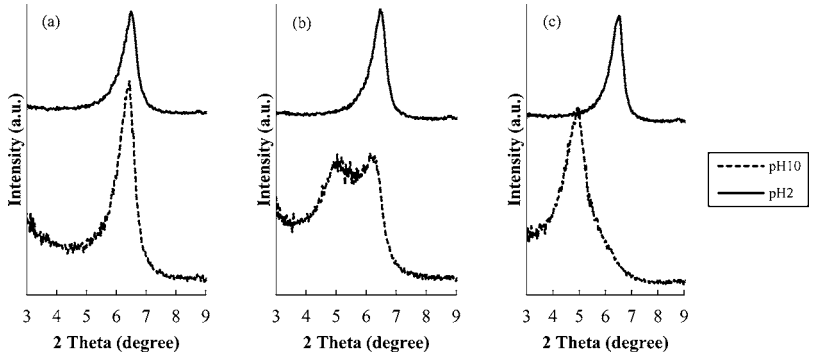

Figure 6. PXRD patterns of (a) G(0.0), (b) G(1.0), and (c) G(2.0)/Na-MMT nanocomposites synthesized in acidic (pH = 2−3) and basic (pH = 10−11) conditions. Reactant ratios for all the nanocomposites were 0.6 g/g PAMAM/Na-MMT.

dx.doi.org/10.1021/ic400198g | Inorg. Chem. 2013, 52, 4603−4610

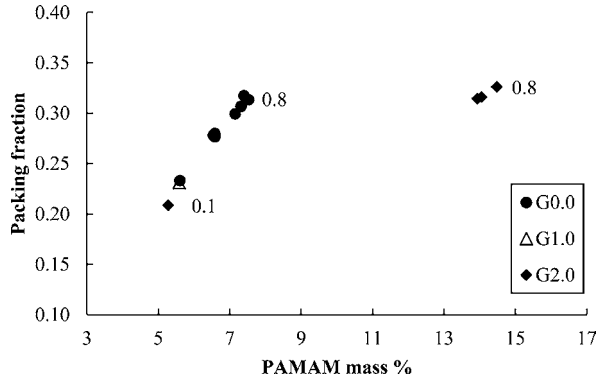

Figure 7. Packing fraction vs dendrimer mass % of nanocomposites synthesized at room temperature and pH 10−11. Labels show reactant ratios (g/g PAMAM/Na-MMT). Packing fractions were not calculated for mixed phases.

although a much lower value can be deduced from data reported for PVOH/Ca-MMT.[6] Linear polymers can yield packing fractions 2−3 times higher than those observed for the PAMAM/Na-MMT nanocomposites. This difference may be due to inefficiencies in packing the flattened dendrimers but may also be an electrostatic effect related to the higher charge density of the dendrimers.

To help understand the mechanism of nanocomposite formation, capillary zone electrophoresis (CZE) was used to evaluate the nature of solvated PAMAM at pH conditions employed in these syntheses. Figure 8 shows electrograms of

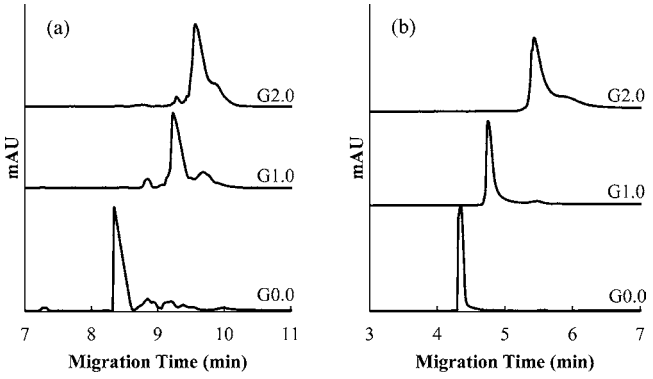

Figure 8. Capillary electrograms for different PAMAM generations at pH 2.7 (a) and 10.9 (b).

PAMAM at pH 2.7 and 10.9, with results summarized in Table 3. The positively charged PAMAM dendrimers migrate toward the cathode under a positive applied voltage. Migration times increase with increasing PAMAM generation, reflecting a decreased charge density for the higher generation dendrimers. Surface charge densities at pH 2.7 were estimated 0.10−0.19 C/m^2. Shi et al.[30] and Ebber et al.[46] also observed clear separation of PAMAM generations 2.0−5.0 at pH 2.5 and generations 1.0−5.0 at pH 2.7. Although these PAMAM generations have similar theoretical charge/mass ratios, Shi et al.[30] proposed a shielding model that retards migration for larger dendrimers.

At pH 10.9, the PAMAM dendrimers (terminal primary amine p$K_a \approx 9-10$)[43−45] are not protonated. However, they may readily coordinate to Na^+ ions in the aqueous solution, forming positively charged complexes. The much faster migration shows that these complexes have higher charge densities than the protonated dendrimers, with calculated surface charges of 0.49−4.5 C/m^2. As in acidic solution, the dendrimer generations show differential shielding and can be separated by migration time.

The differential shielding effects observed for PAMAM generations involve CZE buffer anions, and this mechanism is not necessarily operative under reaction conditions. However, the much higher dendrimer surface charge densities observed in basic aqueous conditions correlates with the faster, higher-yield nanocomposite reactions observed above. On the other hand, more highly charged dendrimers should favor monolayer structures over bilayers, whereas the opposite case was observed. The explanation for this difference may be either that dendrimer complexation within clay galleries is not the same as that in aqueous solution (due to the dramatic conformation change) or that it is related to the reduced MMT surface charge under acidic conditions. The reported ζ potentials and surface charge densities vs pH indicate less negative ζ potential and surface charge density at lower pHs for Na-MMT,[47] bolstering the latter explanation.

Figure 9 and Table 4 compare the FTIR spectra and bond vibrations observed for Na-MMT, PAMAM G(0.0) and a 0.4 PAMAM G(0.0)/Na-MMT nanocomposite. Characteristic bands observed for pristine Na-MMT at 1120 cm^{-1} (Si−O bend), 1048 (Si−O stretch), and 920 (Al−OH stretch) were also present in the nanocomposites without significant shifts, confirming that the aluminosilicate sheets do not change.[48,49] A sharp peak near 3600 cm^{-1} and a broad band at 3400 cm^{-1}, corresponding to O−H stretches, were each present in both Na-MMT and the nanocomposites. The former arises from intrasheet O−H[5,49] and the latter from H_2O adsorbate or intercalate.[49] The latter band, along with the associated O−H bend at 1636 cm^{-1}, are reduced or absent after Na-MMT is

Table 3. Migration Data from CZE and Calculated Charge Data for PAMAM Dendrimers

	pH 2.7			pH 10.9		
	G(0.0)	G(1.0)	G(2.0)	G(0.0)	G(1.0)	G(2.0)
hydrodynamic radius (nm)	0.75	1.10	1.45	0.75	1.10	1.45
ionic strength (mol L^{-1})	0.16	0.16	0.16	0.16	0.16	0.16
average migration time (min)	8.41	9.22	9.66	4.36	4.67	5.45
electrophoretic mobility (m^2/(V·s))	3.87×10^{-8}	3.52×10^{-8}	3.37×10^{-8}	6.21×10^{-8}	5.80×10^{-8}	4.97×10^{-8}
dimensionless mobility	2.82	2.57	2.46	4.46	4.17	3.57
dimensionless ζ potential	3.45	2.94	2.72	10.41	8.80	5.97
ζ potential (V)	0.089	0.076	0.070	0.269	0.227	0.154
charge distribution function (I_0)	8.18	5.59	4.38	192.69	86.05	20.82
surface charge density (C/m^2)	0.192	0.131	0.103	4.526	2.021	0.489

dx.doi.org/10.1021/ic400198g | Inorg. Chem. 2013, 52, 4603−4610

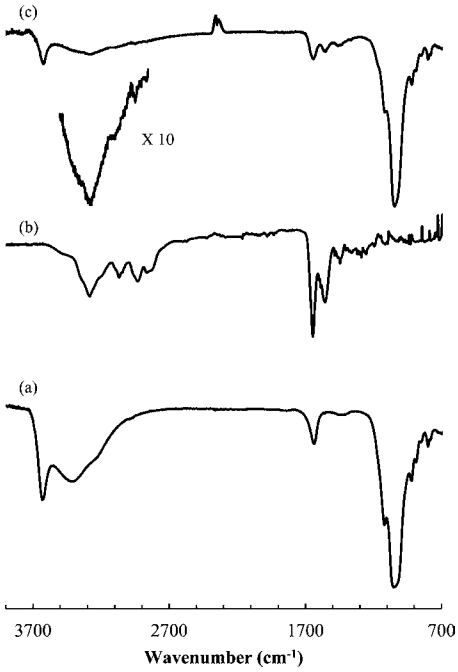

Figure 9. FTIR spectra of (a) NaMMT, (b) PAMAM G(0.0) and (c) 0.4 PAMAM G(0.0)/Na-MMT nanocomposite. The 2850−3500 cm^{-1} region of (c) is intensified x10 for clarity.

Table 4. Comparison of IR Bond Vibrations in Reactants and Nanocomposites

wavenumber (cm^{-1})	PAMAM	Na-MMT	nanocomposites	bond vibration
3600		X	X	O−H str.
3300−3400 (b)		X	X	O−H str.
3300	X		X	N−H asymmetric str.
3000	X		X	N−H symmetric str.
2900	X		X	C−H str.
1640	X		X	amide I (C═O str.)
1635		X	X	O−H bend.
1550	X		X	amide II (N−H bend. + C−N str.)
1120		X	X	Si−O bend.
1045		X	X	Si−O str.
920		X	X	Al−OH str.

heated at 80 °C for 24 h (Figure 2S, Supporting Information). Both O−H absorption intensities are significantly reduced in the nanocomposite, indicating that less water is present in the nanocomposite than in Na-MMT. The terminal amine groups of dehydrated PAMAM G0.0 produce strong N−H stretches at 3284 cm^{-1} (asymmetric) and 3068 (symmetric).[50,51] These absorption intensities increase for higher PAMAM generations, reflecting the larger number of terminal amine groups.[51] The nanocomposites present a band at 3290 cm^{-1} (Figure 9c). The G2.0/Na-MMT nanocomposite (Figure 3S, Supporting Information) shows this band at higher intensity. Characteristic PAMAM absorptions at 2930, 1645, and 1554 cm^{-1}, corresponding to a C−H stretch, amide I (primarily C═O) stretch, and amide II (a combination of N−H in-plane bend and C−N stretch), respectively, are also seen in both dehydrated PAMAM and the obtained nanocomposites.[50]

CONCLUSIONS

Lower generation (G0.0−2.0) PAMAM dendrimers form intercalated nanocomposites with Na-MMT. These are the first reports of the G0.0 and G1.0/Na-MMT nanocomposites and of a structurally ordered G2.0/Na-MMT. Compositional studies show clearly that the structures obtained depend on the generation of PAMAM and the starting organic composition. G0.0 always forms monolayer structures (Δd = 0.42 nm), while G2.0 also forms bilayer structures (Δd = 0.84 nm) at higher organic content, showing a marked monolayer to bilayer transition. G1.0 showed an intermediate behavior, with mixed-phase products obtained at the reactant ratios studied. This monolayer arrangement of PAMAM/clay nanocomposites is reported for the first time. Maximum organic content of G0.0 monolayer and G2.0 bilayer nanocomposites was ∼7% and ∼14% respectively. Although gallery expansions were similar to those observed with linear polymer intercalates, packing fractions of 0.31−0.32 were 2−3 times lower. At acidic pH, the nanocomposites forming only monolayer structures are obtained, indicating a stronger electrostatic attraction between MMT and protonated PAMAM, and these nanocomposites formed more slowly and were more ordered. Na^+ ions play a significant role in nanocomposite formation. At high pH, PAMAMs show high mobility, ζ potential, and surface charge densities due to Na^+ complexation in solution. FTIR data indicates that both Na-MMT and PAMAM structural units are preserved in the nanocomposites obtained.

ASSOCIATED CONTENT

Supporting Information

Comparison of PXRDs for room temperature and 60 °C syntheses and FTIR spectra of dehydrated Na-MMT and 0.4G(2.0)/Na-MMT nanocomposite. This material is available free of charge via the Internet at http://pubs.acs.org.

AUTHOR INFORMATION

Corresponding Author

*Corresponding author. Tel: (+1)-541-737-6747; Fax: (+1)-541-737-2062; E-mail: michael.lerner@oregonstate.edu.

Notes

The authors declare no competing financial interest.

†E.U.I. is a Fulbright visiting scholar, Oregon State University, 2011/12. Permanent address: Department of Chemistry, University of Benin, Benin City, Nigeria.

REFERENCES

(1) Alexandre, M.; Dubois, P. *Mater. Sci. Eng., R* **2000**, *28*, 1−63.
(2) Wu, J. H.; Lerner, M. M. *Chem. Mater.* **1993**, *5*, 835−838.
(3) Lemmon, J. P.; Wu, J. H.; Oriakhi, C.; Lerner, M. M. *Electrochim. Acta* **1995**, *40*, 2245−2249.
(4) Liyanage, A. U.; Lerner, M. M. *RSC Adv.* **2012**, *2*, 474−479.
(5) Oriakhi, C. O.; Nafshun, R. L.; Lerner, M. M. *Mater. Res. Bull.* **1996**, *31*, 1513−1520.
(6) Carrado, K. A.; Thiyagarajan, P.; Elder, D. L. *Clays Clay Miner.* **1996**, *44*, 506−514.
(7) Kanatzidis, M. G.; Bissessur, R.; Degroot, D. C.; Schindler, J. L.; Kannewurf, C. R. *Chem. Mater.* **1993**, *5*, 595−596.
(8) Oriakhi, C. O.; Farr, I. V.; Lerner, M. M. *J. Mater. Chem.* **1996**, *6*, 103−107.
(9) Giannelis, E. P. *Adv. Mater.* **1996**, *8*, 29−35.
(10) Messersmith, P. B.; Giannelis, E. P. *Chem. Mater.* **1993**, *5*, 1064−1066.
(11) Sukpirom, N.; Oriakhi, C. O.; Lerner, M. M. *Mater. Res. Bull.* **2000**, *35*, 325−331.

(12) Huang, J. C.; Zhu, Z. K.; Yin, J.; Qian, X. F.; Sun, Y. Y. *Polymer* **2001**, *42*, 873−877.
(13) Ray, S. S.; Okamoto, M. *Prog. Polym. Sci.* **2003**, *28*, 1539−1641.
(14) Bonczek, J. L.; Harris, W. G.; Nkedi-Kizza, P. *Clays Clay Miner.* **2002**, *50*, 11−17.
(15) Ratanarat, K.; Nithitanakul, M.; Martin, D. C.; Magaraphan, R. *Rev. Adv. Mater. Sci.* **2003**, *5*, 187−192.
(16) Bosman, A. W.; Janssen, H. M.; Meijer, E. W. *Chem. Rev.* **1999**, *99*, 1665−1688.
(17) Tomalia, D. A.; Naylor, A. M.; Goddard, W. A. *Angew. Chem., Int. Ed. Engl.* **1990**, *29*, 138−175.
(18) Kim, Y.; Klutz, A. M.; Jacobson, K. A. *Bioconjugate Chem.* **2008**, *19*, 1660−1672.
(19) Tang, M. X.; Redemann, C. T.; Szoka, F. C. *Bioconjugate Chem.* **1996**, *7*, 703−714.
(20) Singh, P.; Moll, F.; Lin, S. H.; Ferzli, C.; Yu, K. S.; Koski, R. K.; Saul, R. G.; Cronin, P. *Clin. Chem.* **1994**, *40*, 1845−1849.
(21) Zhao, M. Q.; Crooks, R. M. *Adv. Mater.* **1999**, *11*, 217−220.
(22) He, S.; Lin, J. *Appl. Mech. Mater.* **2012**, *108*, 91−94.
(23) Rodlert, M.; Plummer, C. J. G.; Garamszegi, L.; Leterrier, Y.; Grunbauer, H. J. M.; Manson, J. A. E. *Polymer* **2004**, *45*, 949−960.
(24) Alongi, J.; Monticelli, O.; Russo, S.; Camino, G. *J. Nanostruct. Polym. Nanocompos.* **2006**, *2*, 127−133.
(25) Juang, T.-Y.; Chen, Y.-C.; Tsai, C.-C.; Dai, S. A.; Wu, T.-M.; Jeng, R.-J. *Appl. Clay Sci.* **2010**, *48*, 103−110.
(26) Chen, F.; Xiong, H.; Cai, W. W.; Yang, J. T.; Zhong, M. Q. *e-Polym.* **2012**, No. 016.
(27) Rehim, M. H. A.; Youssef, A. M.; Essawy, H. A. *Mater. Chem. Phys.* **2010**, *119*, 546−552.
(28) Wiersema, P. H.; Loeb, A. L.; Overbeek, J. T. *J. Colloid Interface Sci.* **1966**, *22*, 78−99.
(29) Loeb, A. L.; Overbeek, J. T. G.; and Wiersema, P. H. *The Electrical Double Layer around a Spherical Colloid Particle*; MIT Press: Cambridge, MA, 1961.
(30) Shi, X. Y.; Banyai, I.; Lesniak, W. G.; Islam, M. T.; Orszagh, I.; Balogh, P.; Baker, J. R.; Balogh, L. P. *Electrophoresis* **2005**, *26*, 2949−2959.
(31) Zhao, Y. H.; Abraham, M. H.; Zissimos, A. M. *J. Org. Chem.* **2003**, *68*, 7368−7373.
(32) Anthony, J. W.; Bideaux, R. A.; Bladh, K. W.; Nichols, M. C. *Handbook of Mineralogy*; Mineralogical Society of America: Chantilly, VA, 1990.
(33) Amin, A.; Taha, A. S.; El-Ghaffar, M. A. A. *J. Appl. Polym. Sci.* **2010**, *118*, 525−537.
(34) Xie, W.; Gao, Z. M.; Pan, W. P.; Hunter, D.; Singh, A.; Vaia, R. *Chem. Mater.* **2001**, *13*, 2979−2990.
(35) LeBaron, P. C.; Wang, Z.; Pinnavaia, T. J. *Appl. Clay Sci.* **1999**, *15*, 11−29.
(36) Nanjwade, B. K.; Bechra, H. M.; Derkar, G. K.; Manvi, F. V.; Nanjwade, V. K. *Eur. J. Pharm. Sci.* **2009**, *38*, 185−196.
(37) El-Sayed, M.; Kiani, M. F.; Naimark, M. D.; Hikal, A. H.; Ghandehari, H. *Pharm. Res.* **2001**, *18*, 23−28.
(38) Cheng, Y. Y.; Xu, Z. H.; Ma, M. L.; Xu, T. W. *J. Pharm. Sci.* **2008**, *97*, 123−143.
(39) Li, J.; Piehler, L. T.; Qin, D.; Baker, J. R.; Tomalia, D. A.; Meier, D. J. *Langmuir* **2000**, *16*, 5613−5616.
(40) Betley, T. A.; Holl, M. M. B.; Orr, B. G.; Swanson, D. R.; Tomalia, D. A.; Baker, J. R. *Langmuir* **2001**, *17*, 2768−2773.
(41) Hierlemann, A.; Campbell, J. K.; Baker, L. A.; Crooks, R. M.; Ricco, A. J. *J. Am. Chem. Soc.* **1998**, *120*, 5323−5324.
(42) Takada, K.; Diaz, D. J.; Abruna, H. D.; Cuadrado, I.; Casado, C.; Alonso, B.; Moran, M.; Losada, J. *J. Am. Chem. Soc.* **1997**, *119*, 10763−10773.
(43) Castagnola, M.; Zuppi, C.; Rossetti, D. V.; Vincenzoni, F.; Lupi, A.; Vitali, A.; Meucci, E.; Messana, I. *Electrophoresis* **2002**, *23*, 1769−1778.
(44) Brothers, H. M.; Piehler, L. T.; Tomalia, D. A. *J. Chromatogr. A* **1998**, *814*, 233−246.
(45) Cakara, D.; Kleimann, J.; Borkovec, M. *Macromolecules* **2003**, *36*, 4201−4207.
(46) Ebber, A.; Vaher, M.; Peterson, J.; Lopp, M. *J. Chromatogr. A* **2002**, *949*, 351−358.
(47) Delgado, A.; Gonzalezcaballero, F.; Bruque, J. M. *J. Colloid Interface Sci.* **1986**, *113*, 203−211.
(48) Lee, D.; Char, K.; Lee, S. W.; Park, Y. W. *J. Mater. Chem.* **2003**, *13*, 2942−2947.
(49) Sadek, O. M.; Mekhemer, W. K. *Thermochim. Acta* **2001**, *370*, 57−63.
(50) Grabchev, I.; Petkov, C.; Bojinov, V. *Dyes Pigm.* **2004**, *62*, 229−234.
(51) Punyacharoennon, P.; Charuchinda, S.; Srikulkit, K. *J. Appl. Polym. Sci.* **2008**, *110*, 3336−3347.